ATLAS Note

ATL-INT-TILECAL-2019-017

March 1, 2021

Draft version 0.3

Performance of ATLAS Tile Calorimeter Charge Injection System during Run 2

Kathryn Chapman[a], Jim Pilcher[a], Douglas Schaefer[a], Andrew Smith[a], Eleanor Rath[a]

[a]*University of Chicago, Enrico Fermi Institute*

This document is a general overview of the ATLAS Tile Calorimeter's Charge Injection System (CIS) performance during the LHC's Run 2 (2015-2018). A general overview of the calibration system used for the Tile Calorimeter is given. The CIS calibration electronics and data analysis method are then described in detail. Plots used to diagnose CIS stability and performance throughout Run 2 are shown. A description of the software tools used to generate these plots, and other tools used in CIS analysis is given.

Contents

1 Introduction: Tile Calorimeter (TileCal) Calibration

1.1 Tile Calorimeter Calibration

The Tile Calorimeter (alternately referred to as the Hadronic Calorimeter or TileCal in this note) in ATLAS is composed of four cylinders: Long Barrel and Extended Barrel components for both the A and C side of the detector. A cross section of ATLAS displaying the barrels of the TileCal is depicted in Figure 1. Each partition is divided into 64 wedge-shaped modules, and each with space for 48 photomultiplier tubes (PMTs). A cross section of a partition is shown in Figure 2. The scintillatoring tiles in the partition are broken up into cells, and each cell is readout using two PMTs, whose signals are added in towers; this is shown in Figure 3. Long and Extended Barrel modules have different channel mapping, and there are in total 9,852 channels in the whole detector. Each channel has a high and low-gain readout which have an amplification ratio of 64, for a total of 19,704 readouts to be calibrated.

Figure 1: A diagram of the calorimeters of ATLAS, showing the relative positions of the TileCal extended barrel (far left and right) and long barrel (center) partitions.

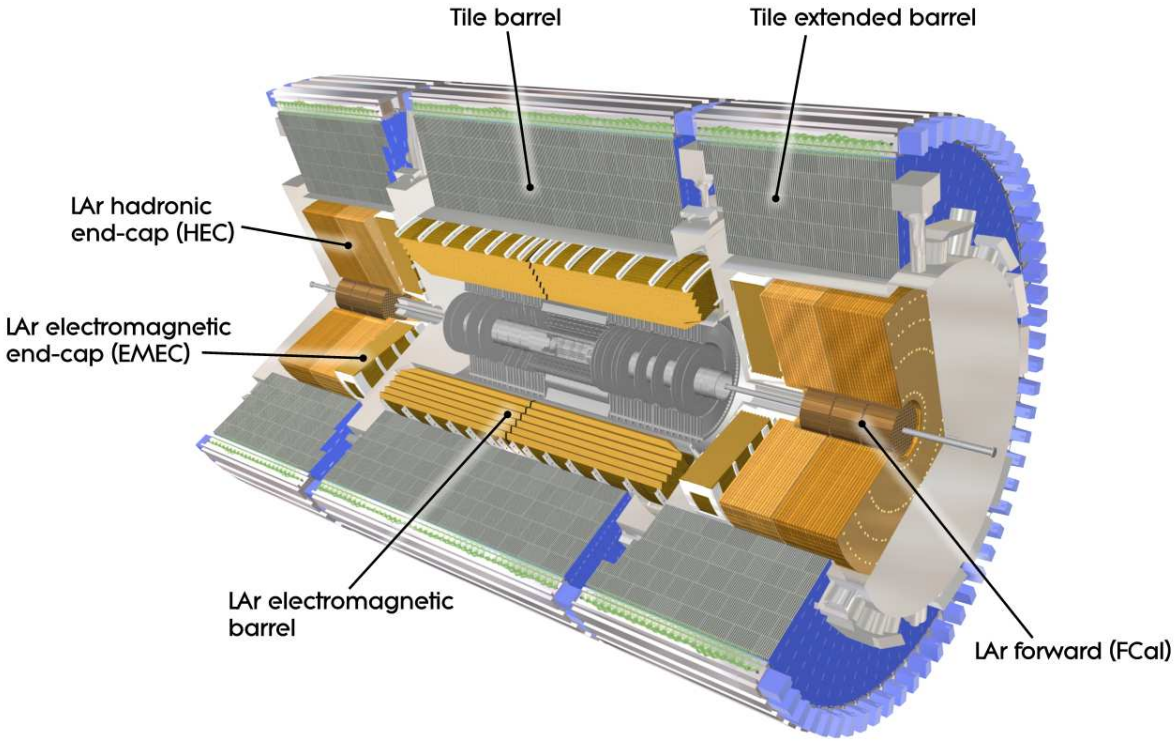

Figure 2: A slice of a TileCal module, showing the layers of scintillating tiles and 8 of the holes where PMTs are placed.

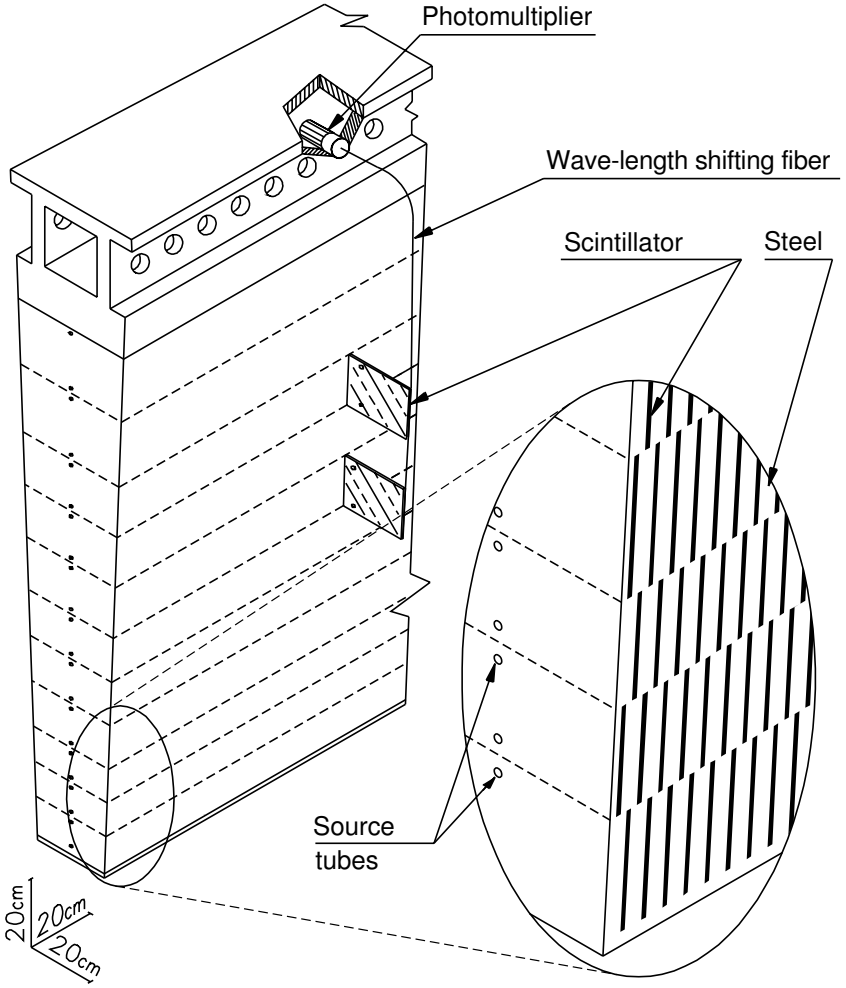

Figure 3: A graphic showing the η coordinates of each cell tower in the Long Barrel and Extended Barrel on one side of the interaction point. For instance, cells A5, BC5 and D2 make up a cell tower with coordinates between $\eta = 0.4$ and $\eta = 0.5$

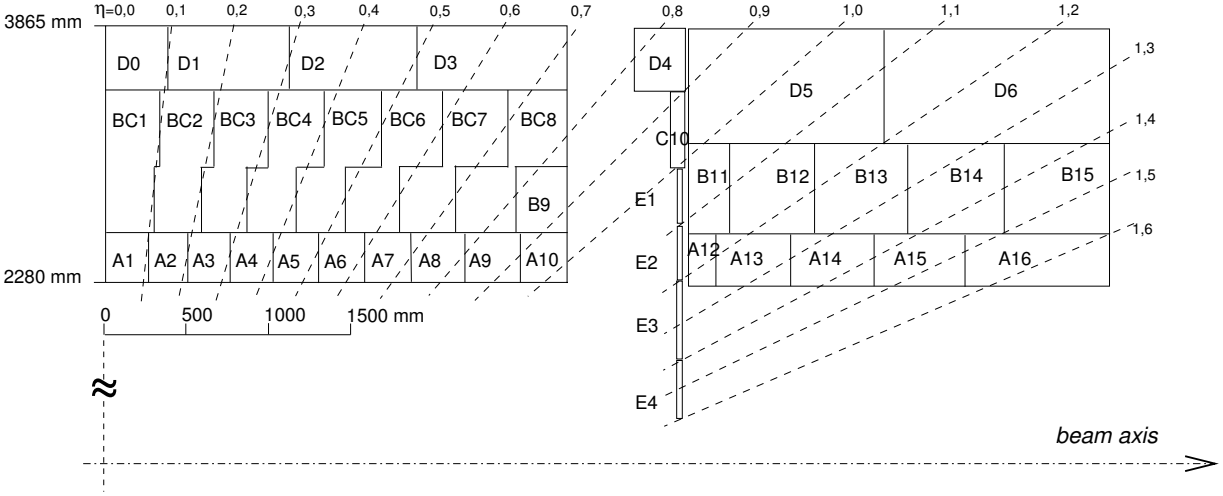

There are three main Tile calibration systems that work together to provide accurate jet energy measurement for the calorimeter. The three calibration systems are: Charge Injection, Laser, and Cesium. Charge Injection calibrates the readout electronics, while Laser calibrates the PMTs and electronics. The Cesium system circulates a radioactive cesium source via hydraulics through the scintillating tiles of each module to calibrate the wavelength shifting fibers, PMTs, and readout electronics at the same time. The combination of the three provides the overall calibration of each readout channel of the detector. Minimum Bias physics events during data taking are used to address changes in response of tile optics over time. Figure 4 explains this calibration chain diagrammatically.

Figure 4: A diagram showing the hierarchy of calibration systems in TileCal

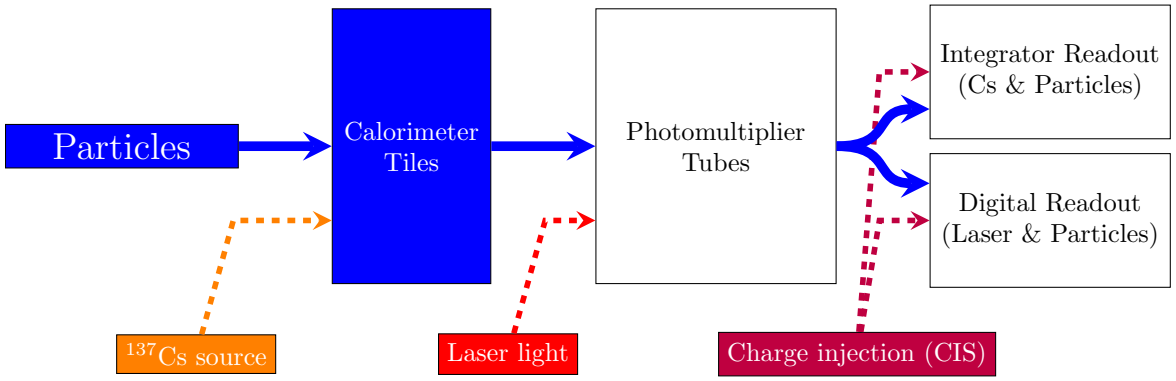

The Charge Injection System (CIS) is controlled by the 3-in-1 cards. The 3-in-1 cards [1] provide a high and low gain shaped output pulses to the digitizer boards, analog trigger output to tower trigger sum boards mounted on the control motherboards, and a slow integrator[1] output used in the Cesium source calibration

[1] An integrator in measurement and control applications is an element whose output signal is the time integral of its input signal.

of the detector. Commands configure the 3-in-1 cards, initiate charge injection, set the integrator gain and DAC calibration, and gate the trigger signal. A source calibration ADC card readout via CANBUS is also mounted on the control motherboards. Fast pulse signals from the 3-in-1 cards are digitized in 8 digitizer boards and sent down a digital pipeline. Each 3-in-1 card uses a 7-pole shaper with shaping time of 50 ns to shape PMT output before digitization. In order to achieve a 16-bit dynamic range using 10-bit ADCs, a bi-gain system is used with a 64:1 gain ratio. The high-gain amplifier has a gain of 32, and the low-gain amplifier has a gain of 0.5. The low gain output has a sensitivity of 2 V/800pC.

The CIS calibration, which is computed from the charge injection on the 3-in-1 cars, consists of the simulation of physics signals through the injection of known charge values into the readout electronics. The relation of the peak amplitude in the response of the electronics (measured in ADC counts) to the value of charge injected (in pico-coulombs) gives the calibration of each ADC in units of ADC counts/pC.

The Laser calibration involves sending laser pulses of known intensities into the PMTs, allowing for calibration with respect to each PMT's response. This allows for the calculation of corrections to the gain linearity and a test for the stability of each PMT over time.

The Cesium calibration consists of circulating sources of ^{137}Cs around the detector. γ-rays of known energy are emitted by this isotope. These photons interact with the plastic scintillating tiles, which then emit photons to the wavelength shifting fibers. This allows for the test of stability and uniformity of the optical response within TileCal cell readout chains. In a Cesium run, the radioactive sources are circulated around Tile using a hydraulic system.

The three calibration systems discussed above are used throughout a data-taking period, and the results are used to keep an up-to-date hadronic calorimeter response. The Laser and CIS calibration runs are taken multiple times per week, while Cesium runs are taken only a few times per year.

In addition to the three physical calibration systems used by TileCal, there are several other monitoring systems. These include Noise (accounting for electronic noise in signal reconstruction), Timing (adjustment of timing in electronics), and EM Scale [2] (converting the calorimeter signals measured as electric charge in pC to the energy deposited by measured electrons which produced the signals[2] (GeV/pC) calibration factor) calibrations extracted from the collected data. Once all calibration systems are taken into account, the energy readout of a channel (in GeV) is given by:

$$E_{\text{channel}}\,[\text{GeV}] = A\,[\text{ADC}] \cdot C_{\text{ADC}\to\text{pC}} \cdot C_{\text{pC}\to\text{GeV}} \cdot \varepsilon_{\text{Cs}} \cdot \varepsilon_{\text{Laser}} \tag{1}$$

where A [ADC] is the signal amplitude A (in ADC counts), $C_{\text{ADC}\to\text{pC}}$ is the CIS calibration factor, $C_{\text{pC}\to\text{GeV}}$ is the EM Scale calibration factor, ε_{Cs} is the Cesium calibration correction factor, and $\varepsilon_{\text{Laser}}$ is the Laser calibration correction factor.

The purpose of this note is to focus on the performance and stability of the Charge Injection System and its calibration over the entirety of Run-2 of the Large Hadron Collider.

1.2 Charge Injection System Overview

As was previously mentioned the Charge Injection System (CIS) works by injecting a fixed charge into the front-end electronics of the Tile Calorimeter in ATLAS in order to simulate a physics signal. The subsequent response of the electronics is measured and compared to the known injected charge in order to determine

[2] This constant of around 1 pC/GeV was fixed during dedicated test beam campaigns.

the relative calibration of a given channel. The Charge Injection System is used in conjunction with Laser and Cesium calibration methods to monitor the response and performance of the Tile Calorimeter.

Each calibration is performed by injecting the electronics of a given module with a full dynamic range of input signals, comparable to what the detector is expected to experience in normal running. The ratio of a given injected charge to the peak response of the electronics is used to determine the CIS constant (ADC counts/pC) of a given readout channel. An accuracy of 1% precision in the calibrations is chosen to align with the design goal of the electronics.

Figure 5: Diagram of the Charge Injection System. Known charge values are injected into the pulse shaping circuit and then read out by both ADCs.

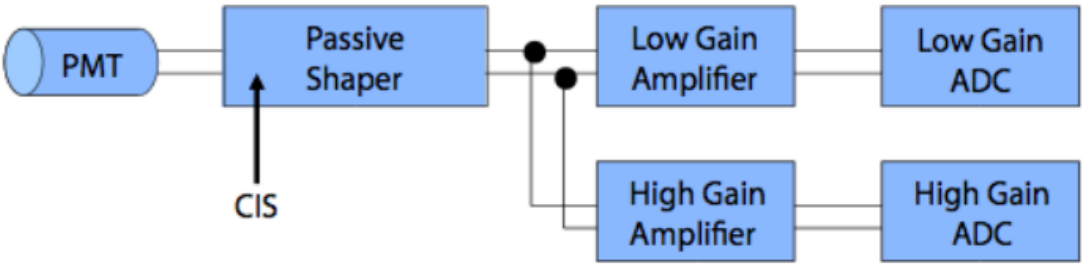

2 Charge Injection System

2.1 Specifics of the CIS

As noted in Section 1, CIS runs are taken roughly every day in ATLAS. During these runs charges of known values are injected by two capacitors in the 3-in-1 card: first by a 5.2 pF capacitor and then a 100 pF capacitor. Currently, only injections from the 100 pF capacitor are used for determining the CIS calibration constants so that the same capacitor is used for the low and high gain amplifiers. A schematic of the charge injection system is shown in Figure 5 The passive pulse shaper produces a pulse shape similar to a Gaussian, with a full width half maximum (FWHM) value of $\approx$ 50 ns. Before traveling to the digitizers, the pulse is split and sent through two separate amplifiers separated by a relative gain of 64. Within the ADCs, each pulse is derived from 7 consecutive samples, with each sample separated by 25 ns. The peak amplitude and phase shift of each pulse readout is estimated by performing a Gaussian fit using the 7 sample values. The first plot in Figure 6 illustrates the digital samples of a CIS event as well as the fitted pulse shape.

The capacitor discharges repeatedly for each charge value as the timing (phase) is varied. For each charge value the timing, i.e. phase, is incremented 15 times in steps of 1.7 ns, and the phase of the injected charge is done with respect to the 40 MHz sampling clock used by ATLAS. Four injections are performed at each phase step, producing 60 events in total for each injected charge. A peak amplitude is extracted for each of the 60 injections of a given charge by the process outlined previously. These fitted Gaussian amplitudes define a distribution of measured charges for each fixed, injected charge. This is illustrated in the middle plot of Figure 6.

The magnitude of each charge is controlled by a 10-bit Digital to Analog Converter (DAC), with a conversion factor of 0.801 pC per DAC setting count. The DAC setting is increased from 0 to 15 with a step size of

1 for the high gain readout, and varied from 32 to 992 with a step size of 32 for the low gain. Together the two readout channels provide a comprehensive test of the electronics response over the full range of energies which are to be expected during regular running of the LHC.

The procedure of injecting charges, sampling the analog pulse, and then measuring the fitted amplitude is repeated as the DAC value is increased. The mean fitted amplitudes are then plotted against the injected charge, yielding a linear relationship between mean fit amplitude (in ADC counts) and injected charge (in pC). For specific ranges of charge (3-10 pC for high gain ADC's, 300-700 pC for low gain ADC's)[3] a single parameter (y = mx) fit is applied[4] The slope of this linear fit then yields a CIS calibration constant for the ADC of each channel in units of ADC/pC.

Figure 6: Overview of a Charge Injection run. 60 injections occur for each DAC setting. The mean of the 60 fitted amplitudes is plotted against the injected charge value. This process is repeated, yielding a linear relationship between fit amplitude (in ADC counts) and injected charge value (in pC) a linear fit to these data is applied, which gives the CIS calibration constant for this ADC and CIS run.

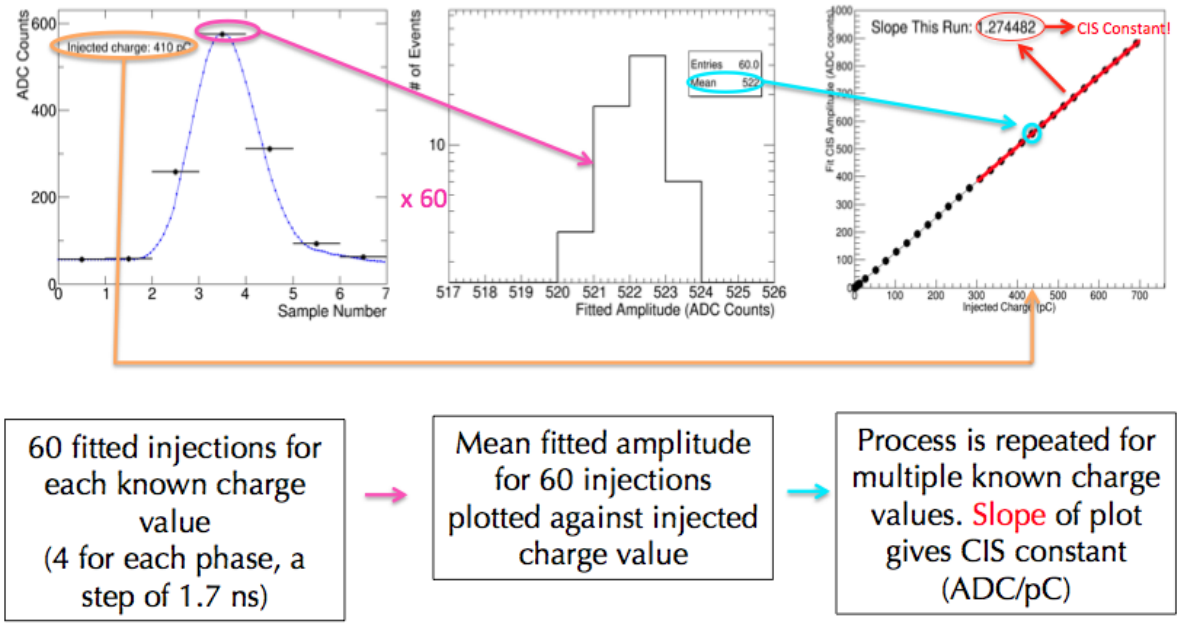

The calculation of the CIS constant is primarily dependent on the amplitude extracted from fitting the pulse shape using a method called "Optimal Filtering", where a known pulse shape[5] is multiplied by a given Gaussian fit amplitude and then shifted in time by the proper phase. The time dependence of an example CIS constants is shown in Figure 7. The measured pedestal value is then added to the pulse in order to shift it to the correct magnitude (ADC sample value >0 when no injection occurs).

[3] The lower limits of each fit range was chosen to ensure the precision of each injection used was at least 0.04%, which ensures a measured error value of less than 0.5%. The upper limit on the high gain fit range eliminates injections that saturate the ADC, as the amplitude of charge values > 10 pC are all read out at 1023 ADC counts in behaving ADC's.

[4] A few small, non-linear factors are incorporated into the fit for low gain ADC's. See Ref. [3]

[5] The pulse shape was determined using test beam data taken during the development of the Tile Calorimeter. The pulse shape data account for the "leakage pulse" a small but non-negligible signal injected into the pulse shaping circuit by the electronic components that charge each capacitor.

Figure 7: Plot of CIS constants vs. time for a single Tile ADC. Each black point represents the measured CIS constant for this ADC for a single CIS calibration run. The blue triangles represent database CIS constant values, which are discussed in Section 3.

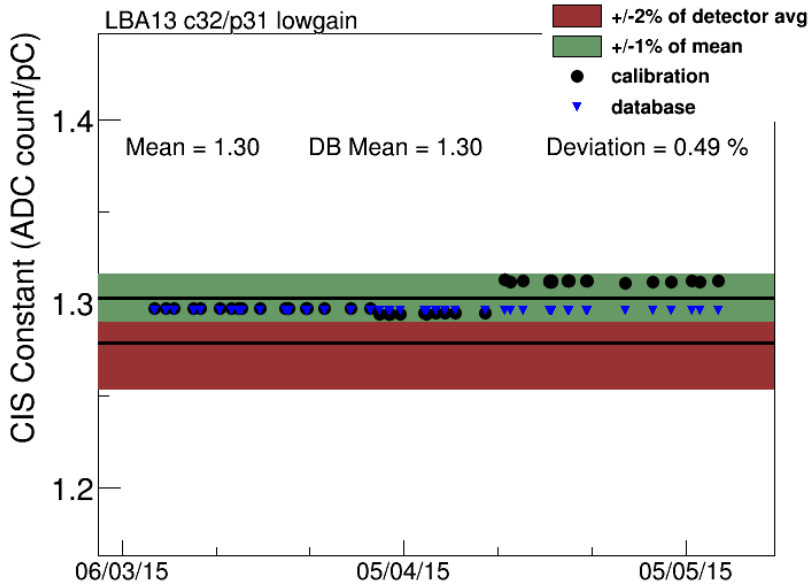

When a Charge Injection run is taken during Run-2 of the LHC two ROOT files are produced. The first file contains raw injection data for each ADC, such as the pulses and the individual CIS Scans. This file can be used to diagnose individual problems. The other file contains data and parameters for the entire calibration and is used during database updates. For more information about how to analyze CIS data, refer to Ref. [3].

2.2 Specifics of Electronics

The Charge Injection System uses two capacitors- one large and one small- with capacitance of 100 pF and 5 pF, respectively. The 10-bit DAC uses a nominal value of 8.192 V, corresponding to 1023 counts while the integrator uses 4.096 V. In order to achieve a 16-bit dynamic range using 10-bit ADCs, a bi-gain system is used with a 64:1 gain ratio. The high-gain amplifier has a gain of 32, and the low-gain amplifier has a gain of 0.5. The low gain output has a sensitivity of 2 V/800 pC.

The absolute energy scale of TileCal is derived by the results of electron testbeam data analysis Ref. [4]. The response of a TileCal module is defined as the ratio of the charge collected in the calorimeter cell divided by the electron beam energy. More than 200 cells of the first radial sample were analyzed and the average energy scale is of 1.05 pC/GeV with an RMS of 2.4%.

Combining the above values for the 100 pC capacitance gives a conversion factor of 0.801 pC / ADC count, calculated below.

$$\begin{aligned}\text{Accumulated charge in a capacitor} &= \text{Capacitance} \times \text{Voltage}\\ Q_{\text{acc}} &= (100\text{pF}) * (8.192\text{V})\\ \text{Accumulated charge/ADC counts} &= Q_{\text{acc}}/1023 = 819.2\ \text{pC}/1023\ \text{ADC counts}\end{aligned}$$

More information on the calculation and uncertainties of these values can be found in Ref. [5, 6].

3 Performance and Stability of CIS During Run-2

As was stated earlier CIS calibration runs were taken on a daily to weekly basis for the entirety of Run-2 of the LHC. During normal running these calibration runs were analyzed individually to extract CIS constants and diagnose problematic channels. In addition to this day-to-day analysis of CIS Run Data, studies on the performance and stability of generated constants were compiled on a yearly basis. In the sections below, plots demonstrate the performance of various aspects of the CIS system are reproduced for each year of Run-2. Additionally, a set of summary plots containing data over the full range of Run-2 (2015-2018) are included.

3.1 Detector Time Stability

Figures 8, 9, 10, and 11 each show the detector-wide CIS calibration constant averages of all the high-gain (HG) and low-gain (LG) ADCs for a selection of CIS calibrations from a single year during Run-2. A selection of CIS calibration runs spanning Run-2 is shown in Figure 12. In each CIS calibration, there is a 0.7% systematic uncertainty present in individual calibrations, represented by the yellow error band. This uncertainty comes from the observed peak output amplitudes and is taken as characteristic of the channel-to-channel variation from this source, prior to any calibration. From the data shown, it is clear that the detector-wide mean CIS constant over all non-problematic channels falls within the systematic error band of the typical channel plotted, throughout Run-2.

Figure 8: Detector-wide CIS calibration constant averages of all the high-gain (left) and low-gain (right) ADCs for a selection of CIS calibration runs between August 2015-October 2015, plotted as black circles. The CIS constants from a typical channel (LBC20, Channel 35 for HG; LBC20, Channel 33 for LG) are additionally plotted as blue triangles for comparison. The RMS values on the plots are indicative of the fluctuation present in calibrations. In addition, there is a 0.7% systematic uncertainty present in individual calibrations, represented by the yellow error band. This uncertainty comes from the observed peak output amplitudes and is taken as characteristic of the channel-to-channel variation from this source, prior to any calibration. Problematic channels are not included when calculating the mean.

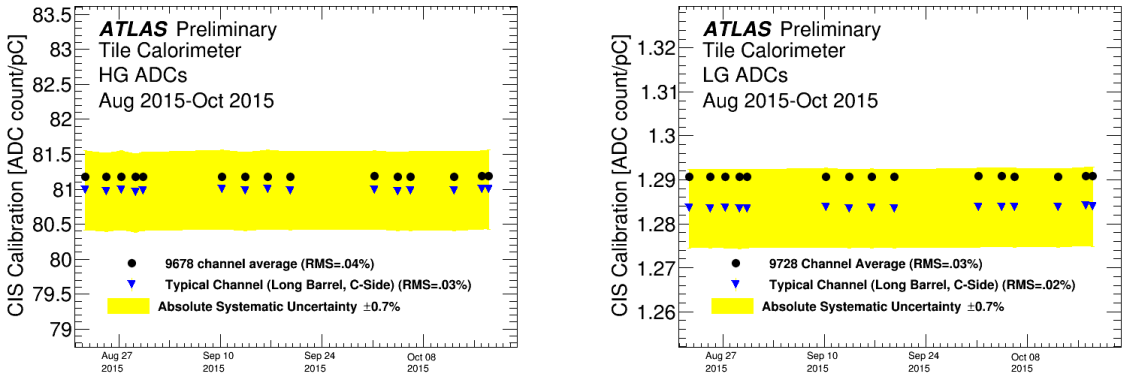

Figure 9: Detector-wide CIS calibration constant averages of all the high-gain (left) and low-gain (right) ADCs for a selection of CIS calibration runs between April 2016-November 2016, plotted as black circles. The CIS constants from a typical channel (LBC20, Channel 35 for HG; LBC20, Channel 33 for LG) are additionally plotted as blue triangles for comparison. The RMS values on the plots are indicative of the fluctuation present in calibrations. In addition, there is a 0.7% systematic uncertainty present in individual calibrations, represented by the yellow error band. This uncertainty comes from the observed peak output amplitudes and is taken as characteristic of the channel-to-channel variation from this source, prior to any calibration. Problematic channels are not included when calculating the mean.

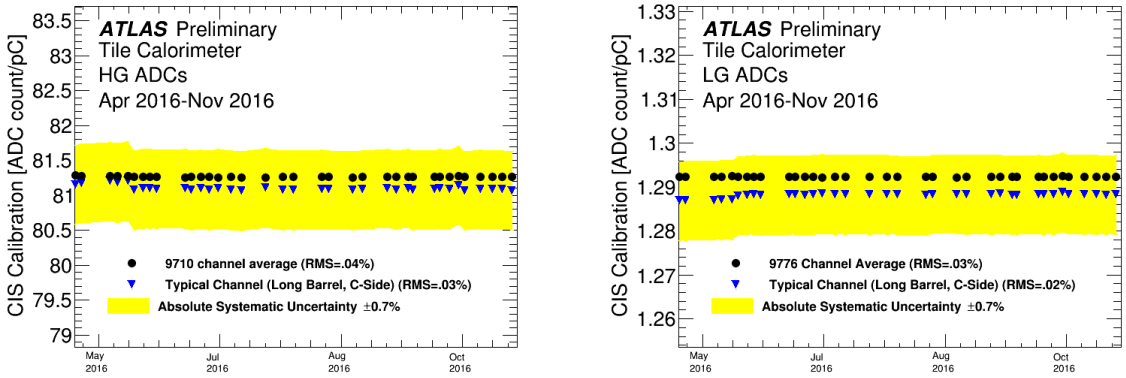

Figure 10: Detector-wide CIS calibration constant averages of all the high-gain (left) and low-gain (right) ADCs for a selection of CIS calibration runs between May 2017-November 2017, plotted as black circles. The CIS constants from a typical channel (LBC20, Channel 35 for HG; LBC20, Channel 33 for LG) are additionally plotted as blue triangles for comparison. The RMS values on the plots are indicative of the fluctuation present in calibrations. In addition, there is a 0.7% systematic uncertainty present in individual calibrations, represented by the yellow error band. This uncertainty comes from the observed peak output amplitudes and is taken as characteristic of the channel-to-channel variation from this source, prior to any calibration. Problematic channels are not included when calculating the mean.

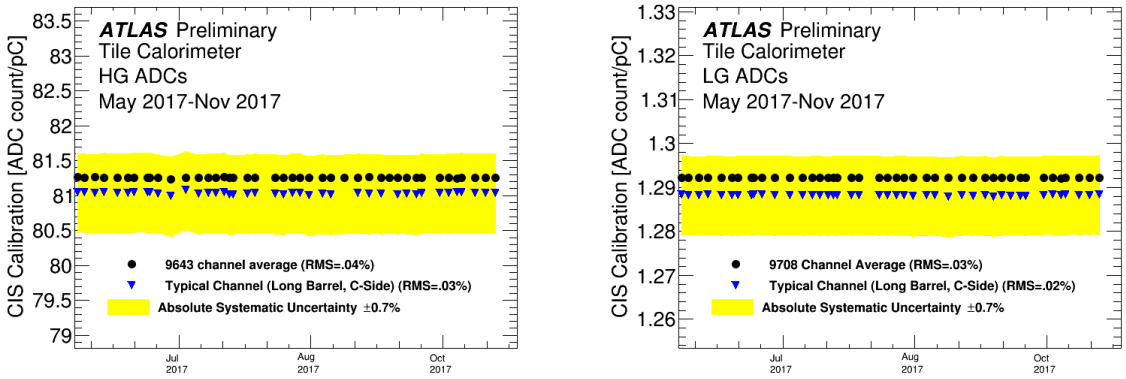

Figure 11: Detector-wide CIS calibration constant averages of all the high-gain (left) and low-gain (right) ADCs for a selection of CIS calibration runs between April 2018-December 2018, plotted as black circles. The CIS constants from a typical channel (LBC20, Channel 35 for HG; LBC20, Channel 33 for LG) are additionally plotted as blue triangles for comparison. The RMS values on the plots are indicative of the fluctuation present in calibrations. In addition, there is a 0.7% systematic uncertainty present in individual calibrations, represented by the yellow error band. This uncertainty comes from the observed peak output amplitudes and is taken as characteristic of the channel-to-channel variation from this source, prior to any calibration. Problematic channels are not included when calculating the mean.

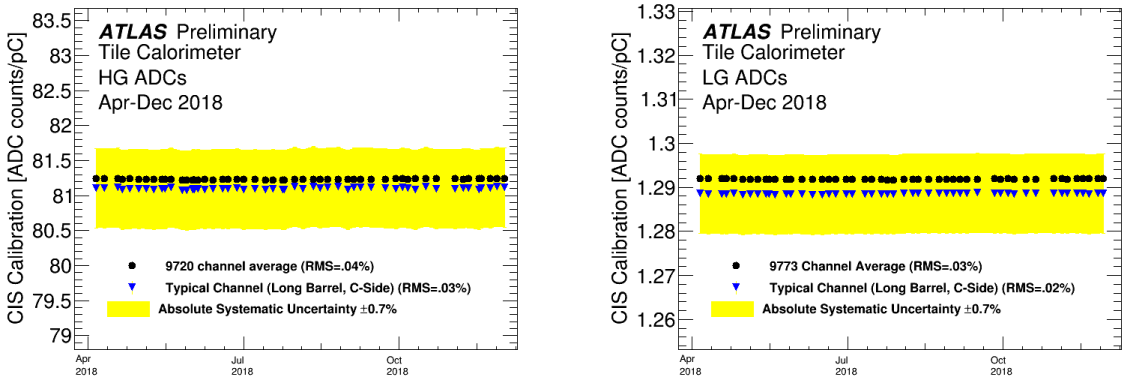

Figure 12: Detector-wide CIS calibration constant averages of all the high-gain (left) and low-gain (right) ADCs are shown for a selection of CIS calibration runs between August 2015-November 2018. The calibration points are plotted as black circles. The CIS constants from a typical channel (LBC20, Channel 35 for HG; LBC20, Channel 33 for LG) are additionally plotted as blue triangles for comparison. The RMS values on the plots are indicative of the fluctuation present in calibrations. In addition, there is a 0.7% systematic uncertainty present in individual calibrations, represented by the yellow error band. This uncertainty comes from the observed peak output amplitudes and is taken as characteristic of the channel-to-channel variation from this source, prior to any calibration. Problematic channels are not included when calculating the mean.

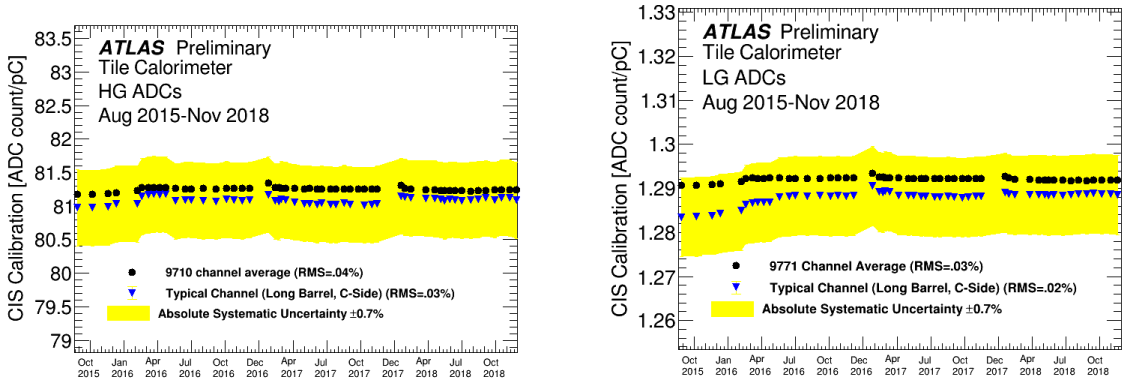

3.2 CIS Constant History

Figures 13, 14, 15, and 16 show the percent change in detector-wide CIS constants between two months in a selected year during Run-2. Figure 17 shows the percent change in the average CIS constant for every channel in the detector between August 2015 (at the onset of Run-2) and October 2018 (at the end of Run-2). In all figures shown, channels that are unresponsive or have CIS constants which fluctuate run-to-run are not included. From Figure 17, it is clear that in the duration of Run-2 the CIS constants of less than 50 channels in the detector changed by more than ±4%.

Figure 13: Percent change in detector-wide CIS constants between August 2015-October 2015. The RMS variation is approximately 0.05%. Channels that are unresponsive or have fluctuating CIS constants are not included.

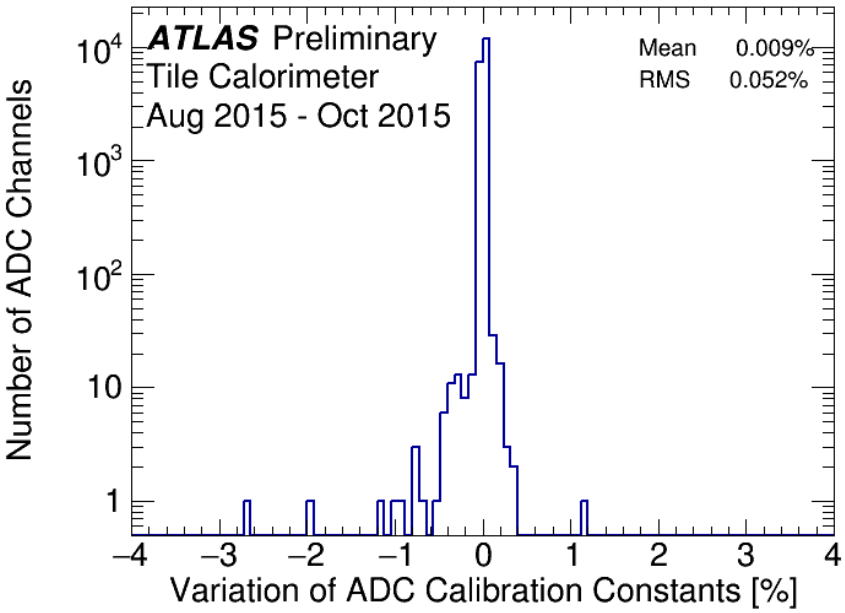

Figure 14: Percent change in detector-wide CIS constants between May 2016-November 2016. The RMS variation is approximately 0.10%. Channels that are unresponsive or have fluctuating CIS constants are not included.

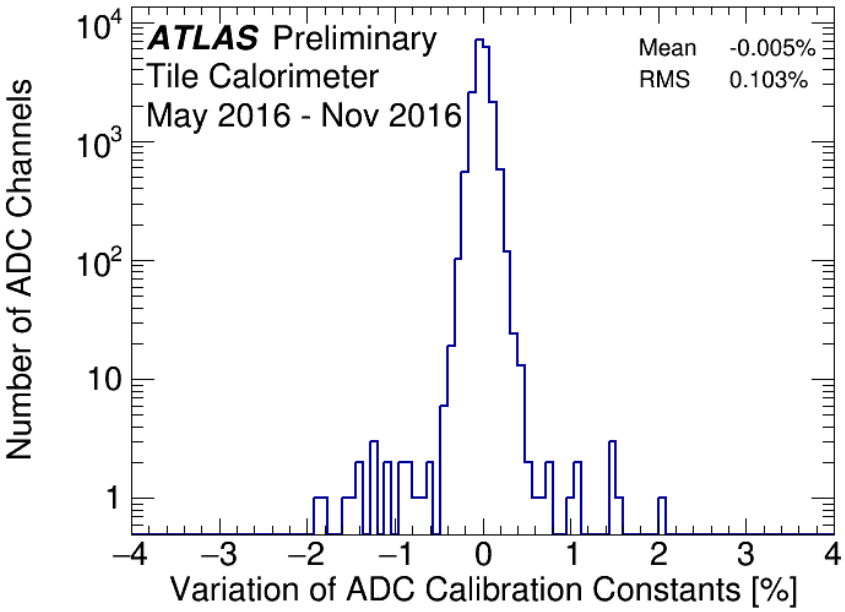

Figure 15: Percent change in detector-wide CIS constants between June 2017-October 2017. The RMS variation is approximately 0.07%. Channels that are unresponsive or have fluctuating CIS constants are not included.

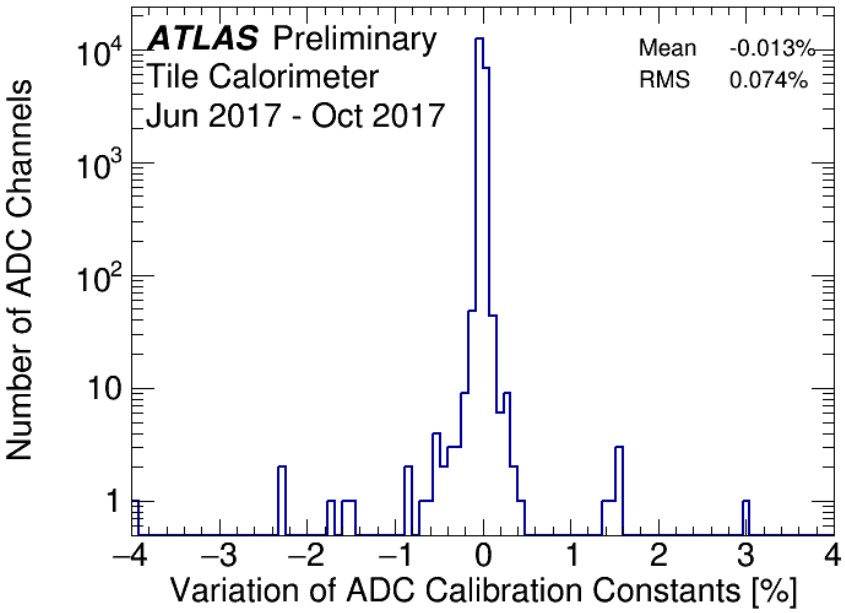

Figure 16: Percent change in detector-wide CIS constants between April 2018-November 2018. The RMS variation is approximately 0.06%. Channels that are unresponsive or have fluctuating CIS constants are not included.

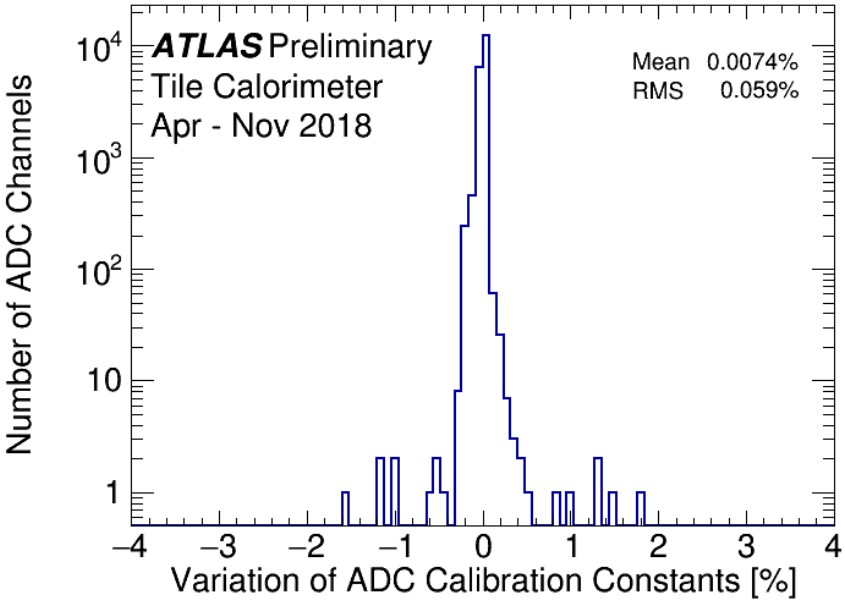

Figure 17: Percent change in detector-wide CIS constants between August 2015-October 2018. The RMS variation is approximately 0.35%. Channels that are unresponsive or have fluctuating CIS constants are not included.

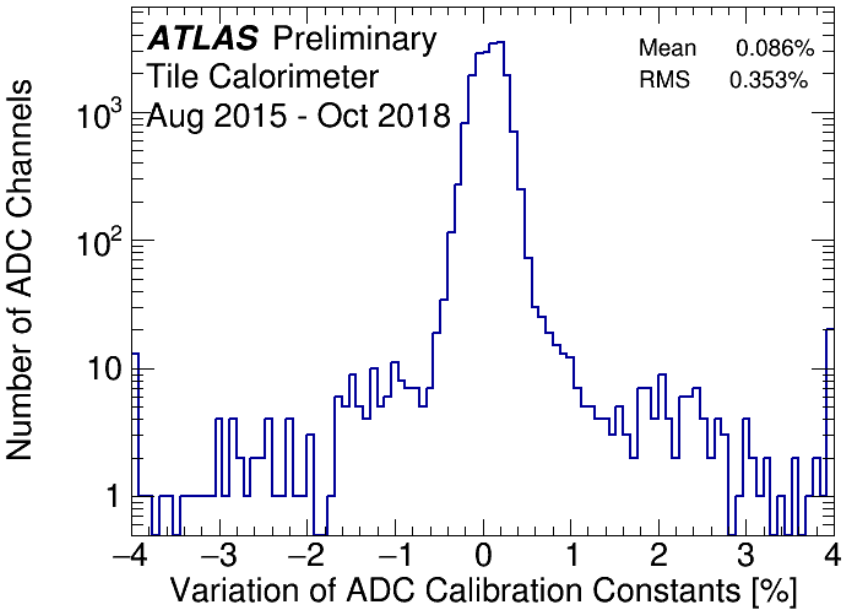

3.3 CIS Distribution

Figures 18, 19, 20, and 21 show the distribution of the CIS calibration constants over each year of Run-2, for all the low-gain (LG) and high-gain (HG) channels in the detector. Typical variation is approximately 1.6% in both gains for both gains. In addition, the systematic uncertainty is 0.7% for the calibration constants of individuals channels. Channels that are unresponsive or have fluctuating CIS constants are not included.

Figure 18: Distribution of the average low gain (left) and high gain (right) CIS constants for all CIS calibration runs taken between August 21st and October 21st of 2015. The distribution is approximately normal with an RMS/mean ratio in both gains of 1.6%.

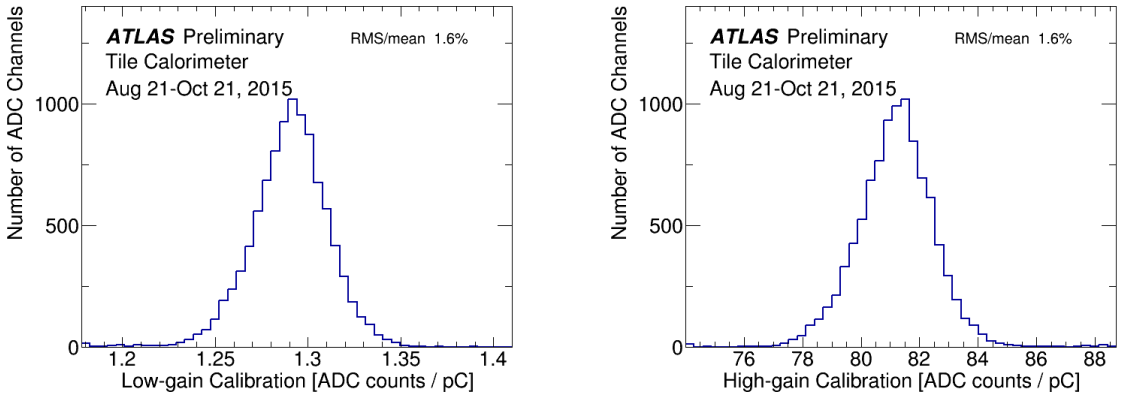

Figure 19: Distribution of the average low gain (left) and high gain (right) CIS constants for a standard CIS calibration run taken on October 2, 2016. The distribution is approximately normal with an RMS/mean ratio in both gains of 1.6%.

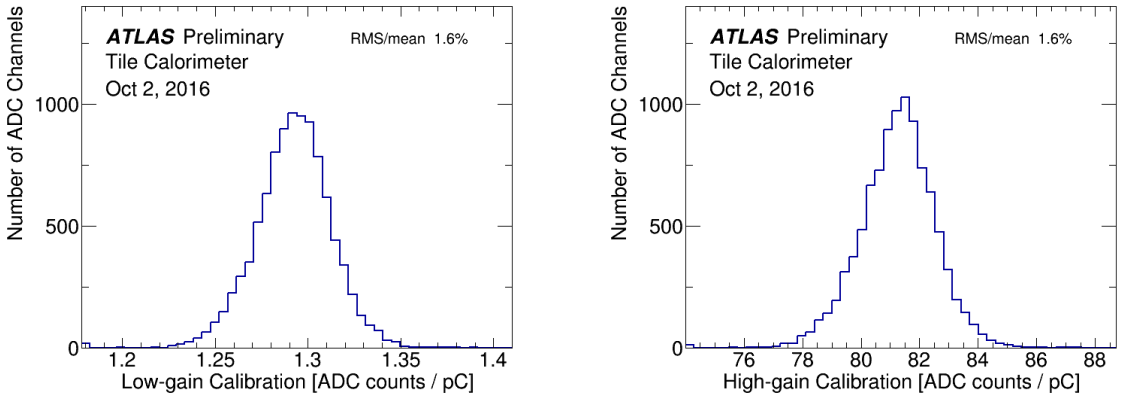

Figure 20: Distribution of the average low gain (left) and high gain (right) CIS constants for a standard CIS calibration run taken on November 12th, 2017. The distribution is approximately normal with an RMS/mean ratio in both gains of 1.6%.

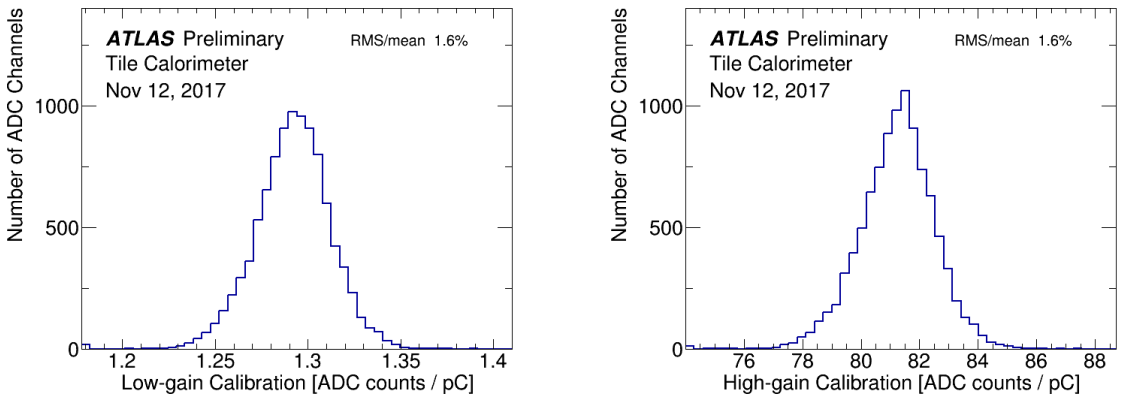

Figure 21: Distribution of the average low gain (left) and high gain (right) CIS constants for all CIS calibration runs taken during November of 2018. The distribution is approximately normal with an RMS/mean ratio in both gains of 1.6%.

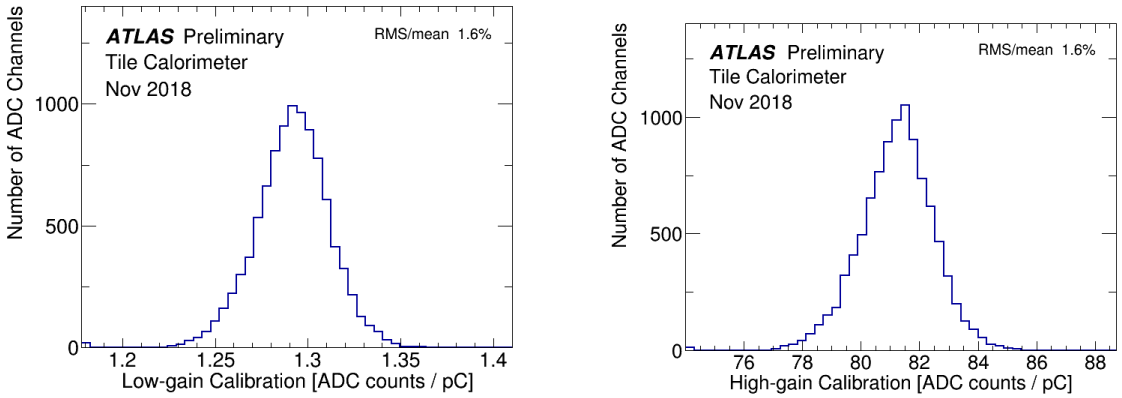

3.4 ADC Status Time Stability

Figure 22 shows the number of ADCs failing in each status category throughout Run-2. The status categories are stored in a database, which we call the COOL database. It is primarily used for storing detector conditions data, but also status flags which are uploaded summaries of information to indicate the detector reliability during a run. Further discussion is given in Section 4.1. Downward fluctuations in the number of ADCs failing any quality criteria at the start of each calendar year correspond to periods of detector maintenance. The categories, which are called flags, include the following:

- "BadCIS" flag: An ADC that is not returning a charge constant within the design specifications but is returning a non-zero value.
- "NoCIS" flag: These are ADCs that do not respond. Often due to an over-current that destroys the digitizer card. This happens at a very low rate.
- "Masked" due to CIS: These are ADCs that are problematic due to errors that result in the channel needing to be masked. Problems could be from electronic noise or other issues.
- "Masked for any reason": These are ADCs could not be readout. Most of these come from entire modules losing cooling or other problems that result in the loss of operation. Typically these are fixed at the beginning of the year during the maintenance period where the number of masked channels are small.

Figure 22: This scatter plot shows the number of ADCs with CIS-related failures in the COOL database for a selection of CIS calibration runs spanning Run-2. During a given run, channels with the "No CIS" flag showed no CIS response and channels with the "Bad CIS" flag showed an RMS/mean ratio > 4% in the linear fit performed to obtain a CIS constant for the run. Note that as channel status in COOL are updated less frequently than calibration runs occur, many consecutive runs have identical numbers of channels with each status.

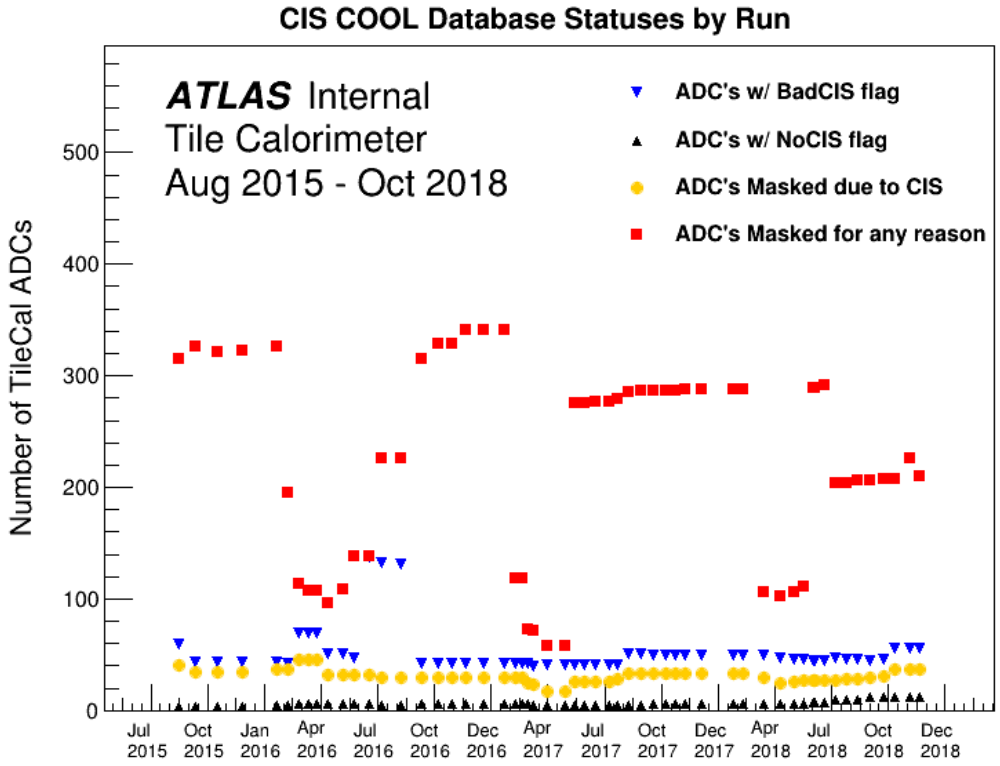

3.5 CIS TUCS Flag Plots

The histograms in Figures 23, 24, 25, and 26 show the number of ADCs failing select TileCal Unified Calibration Software (TUCS) Quality Flags for 2015, 2016, 2017, and 2018 data taking years, respectively. TUCS is a software package that contains the main tools for analyzing CIS calibration run, and it is described further in Section 4. The flag status for each channel are calculated using the definitions listed in Table 1. The number of ADCs failing on at least one flag in a given run is plotted as red triangles. Throughout Run-2, the number of ADCs in this category remains lower than 5% of all channels in the detector, an indicator of the CIS stability during this time period.

Figure 23: Scatter plot showing the number of ADCs failing each TUCS Quality Flag between August 2015-October 2015. The definitions of each flag name shown in the legend can be found in Table 1.

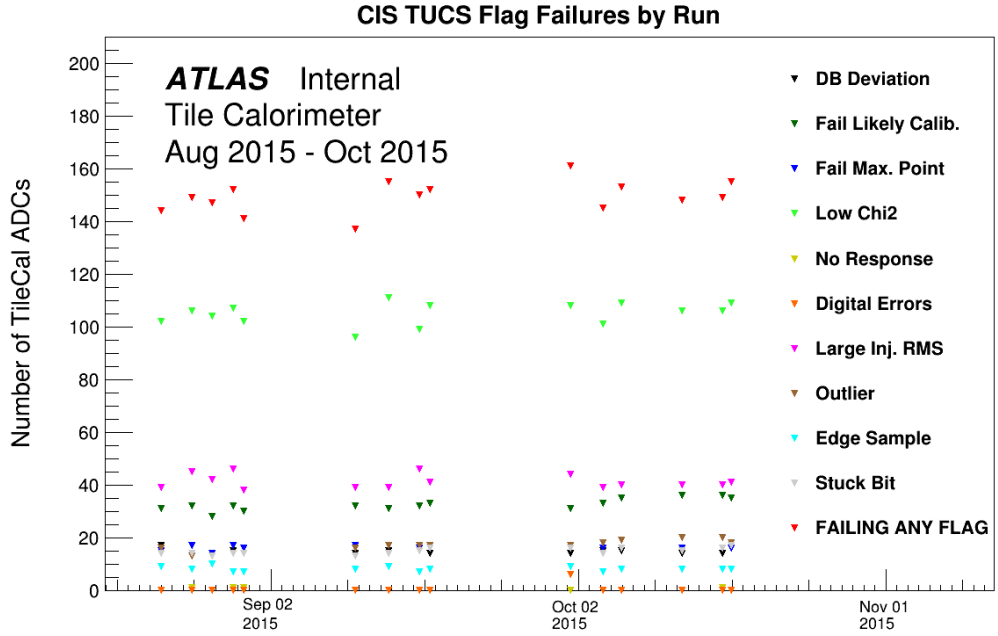

Figure 24: Scatter plot showing the number of ADCs failing each TUCS Quality Flag between April 2016-November 2016. The definitions of each flag name shown in the legend can be found in Table 1.

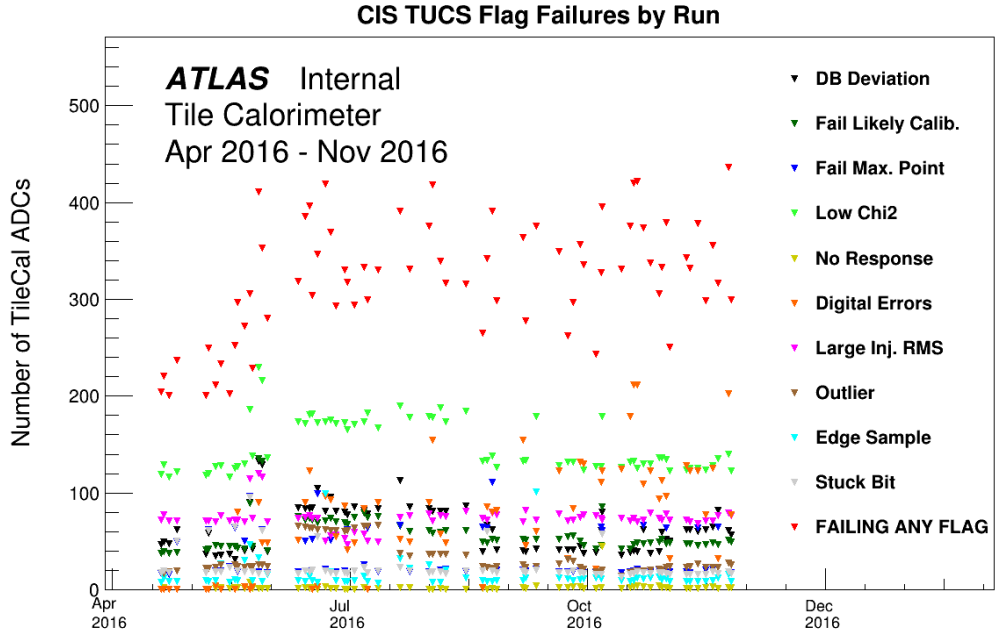

Figure 25: Scatter plot showing the number of ADCs failing each TUCS Quality Flag between May 2017-December 2017. The definitions of each flag name shown in the legend can be found in Table 1.

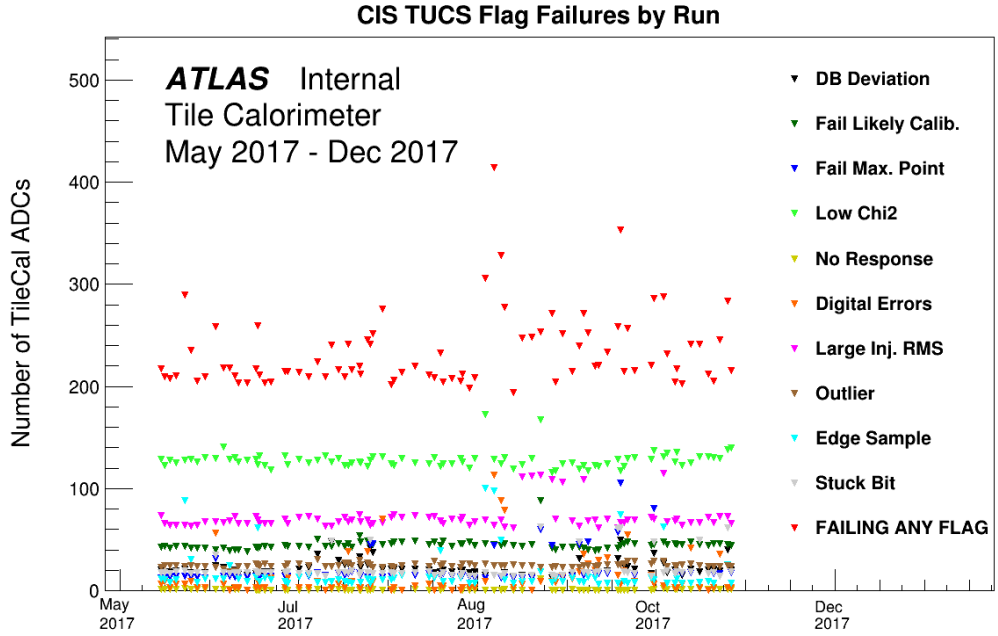

Figure 26: Scatter plot showing the number of ADCs failing each TUCS Quality Flag between April 2018-October 2018. The definitions of each flag name shown in the legend can be found in Table 1.

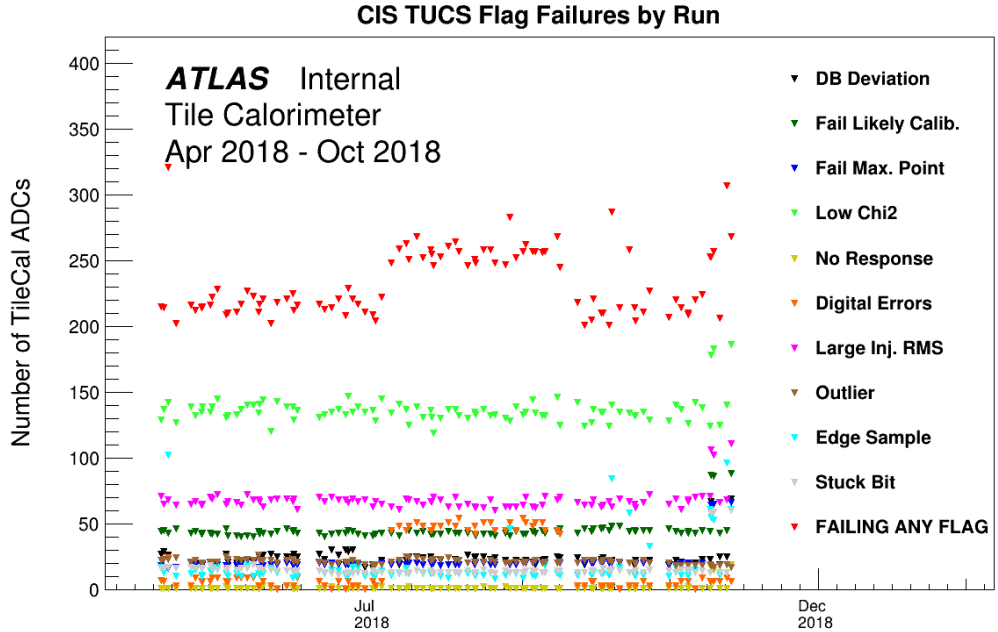

3.6 CIS Calculation RMS

The histograms in Figures 27, 28, 29, and 30 show the ratio of CIS constant RMS to mean for all channels, both high-gain (HG) and low-gain (LG), in the detector for a time period selected from each year during Run-2. Figure 31 shows the same information for a selection of CIS calibration runs which span all years of Run-2. Channels that are unresponsive or fail certain TUCS quality flags are not included. This plot shows that the number of channels whose CIS linear fit RMS is ≥ to 1.0% of the computed CIS constant is on the order of 100 channels in both high gain and low gain for all of Run-2.

Figure 27: The ratio of CIS constant RMS to mean for all channels, both high-gain (HG) and low-gain (LG), in the detector for the time period between August 2015-October 2015. Overflow is included in the rightmost bin of both histograms. Channels that are unresponsive or show certain TUCS quality flags are not included.

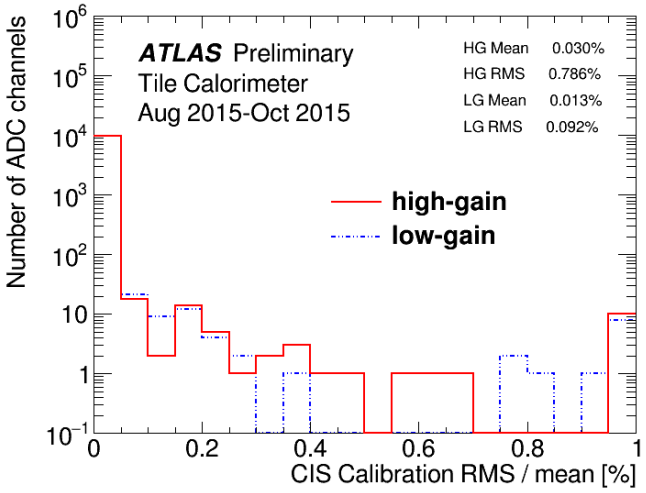

Figure 28: The ratio of CIS constant RMS to mean for all channels, both high-gain (HG) and low-gain (LG), in the detector for the time period between April 2016-November 2016. Overflow is included in the rightmost bin of both histograms. Channels that are unresponsive or show certain TUCS quality flags are not included.

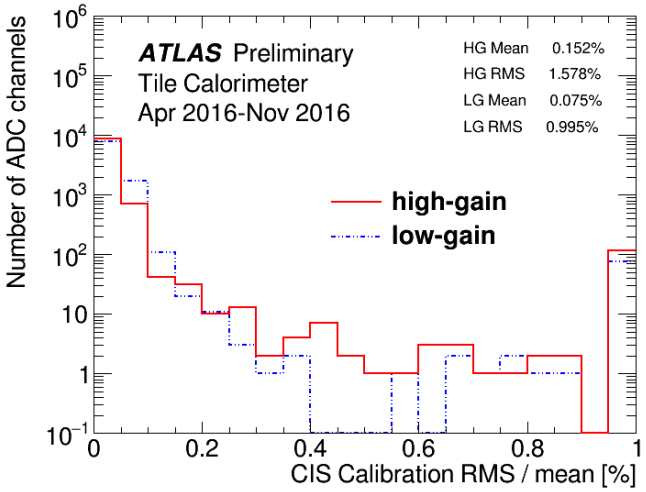

Figure 29: The ratio of CIS constant RMS to mean for all channels, both high-gain (HG) and low-gain (LG), in the detector for the time period between May 2017-December 2017. Overflow is included in the rightmost bin of both histograms. Channels that are unresponsive or show certain TUCS quality flags are not included.

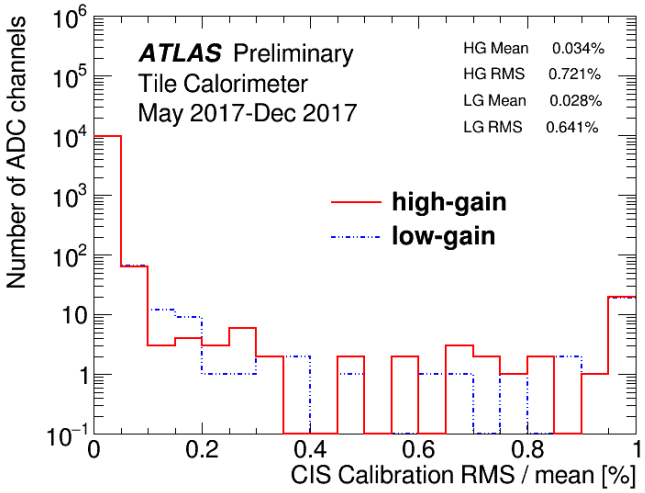

Figure 30: The ratio of CIS constant RMS to mean for all channels, both high-gain (HG) and low-gain (LG), in the detector for the time period between April 2018-November 2018. Overflow is included in the rightmost bin of both histograms. Channels that are unresponsive or show certain TUCS quality flags are not included.

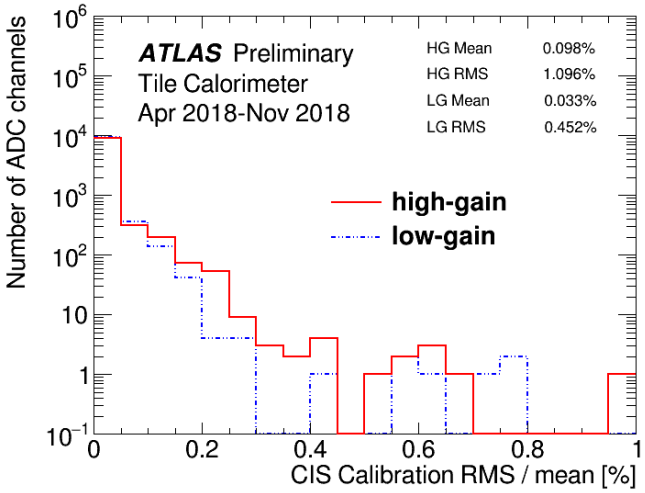

Figure 31: The ratio of CIS constant RMS to mean for all channels, both high-gain (HG) and low-gain (LG), in the detector for the time period between August 2015-November 2018, spanning all of Run-2. Overflow is included in the rightmost bin of both histograms. Channels that are unresponsive or show certain TUCS quality flags are not included.

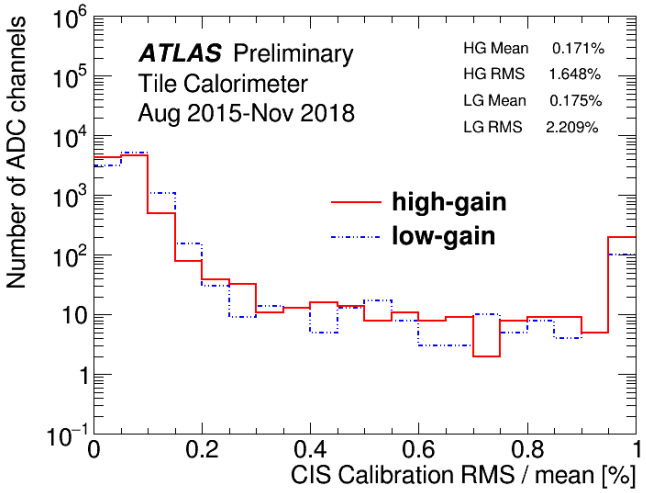

4 CIS Analysis Tools and Software

On a monthly basis the CIS Experts perform a Status Update Procedure as detailed in Ref. [7]. The CIS flagging procedure is used in reevaluating problematic channels, updating the values of channel-by-channel calibration constants in the database, and generally assessing the performance and stability of the CIS system of the Tile Calorimeter over time. The TileCal Unified Calibration Software (TUCS) is a software package that contains the main tools for analyzing CIS calibration runs.

A CIS update involves plotting the CIS constants for all runs taken in the past month approximately (30-40 days) and plotting them over time for each individual channel. These graphs are then used to 1) assess CIS stability over time 2) calculate an average constant for this time period 3) compare the CIS constant to detector-wide averages to determine if the channel has a reasonable calibration. If a channel has an average constant that has changed significantly (>2%) since the past month the database is updated to reflect this new value. If the channel appears to be stable over the month and within the standard distribution from the detector average no further action is taken to update the calibration in the COOL database as described in Section 4.1.

If instead the channel is problematic, e.g. significant instability and variation in CIS constants between successive runs (variation over the month is >10% of detector average), far from the detector average (>5% separation from the detector average), or lacking data points (no recorded CIS constant or a CIS constant of 0 for multiple runs) then further action is taken to mark the channel as problematic. In extreme cases the channel may even have to be removed from further calibration entirely. For more information on this process refer to the next section.

4.1 COOL ADC/Channel Status Flags

When issues with problematic Tile ADCs or channels are noticed, they are assigned "Status Flags" in the COOL database [7]. The status flags can apply to a single ADC or to an entire channel, thereby applying to both ADCs pertaining to the channel. Some status are assigned only for minor problems (e.g. RMS variation) and do not prevent data from the ADC or channel from being used. Status flags for more serious problems (e.g. missing data or no calibration recorded) "mask" the ADC or channel, meaning it cannot be used for data analysis, trigger decisions, etc. Figures 23, 24, 25, and 26 show the evolution of CIS flags for all channels in the detector during each year of Run-2.

The Python scripts that read and write information to the COOL database assign the term "affected" to channels or ADCs with marked lesser flags, and the term "bad" to channels or ADCs which have problems which require them to be masked. The CIS Experts then prepare an sqlite file to update the COOL database to reflect the recent change in channel status. All changes to the database and channel classification, masking in particular, are discussed with the other calibration experts in the weekly calibration meeting. The decision to label a channel as bad or mask it often requires there to be significant errors in other calibration systems and not just the charge injection system.

Table 1: Qualitative descriptions of CIS TUCS Quality flags. TUCS quality flags are a set of 14 tests that each ADC is subjected to for each CIS run. These tests give a general idea of the overall performance of the ADC. Information on 9 of these tests is stored in the qflag variable, while the rest are determined by worker scripts in TUCS.

TUCS Quality Flags

Flag	Flag Location	Passed if...
No Response	qflag bit 1	At least one successful injection readout
Fail Likely Calib.	qflag bit 3	CIS constant within 6.23% of detector-wide mean
Fail Max. Point	qflag bit 4	$\geq$ 1 point in fit range > 600 ADC counts
Large Injection RMS	qflag bit 5	RMS of all fixed-charge injections in fit range < 5
Digital Errors	qflag bit 6	All digital error checks passed
Low Chi2	qflag bit 7	Linear fit $\chi^2 > 2 \times 10^{-6}$
Edge Sample	qflag bit 8	No events in fit range w/ 1st or 7th sample as max
Next to Edge Sample	qflag bit 9	No events in fit range w/ 2nd or 6th sample as max
Stuck Bit	qflag bit 10	No stuck bits in readout chain detected
Unstable	TUCS	ADC CIS const. RMS/Mean < 0.39%
Mean Deviation	TUCS	CIS constant within 5% of ADC time period avg.
Default Calibration	TUCS	Default CIS constant not used in database
Outliers	TUCS	CIS const. < 6 and > 15% away from det. avg.
DB Deviation	TUCS	Measured and database const. differ by < 1%

Table 2: Qualitative descriptions of COOL status flags.

ADC Status Flags

Flag	Flag#	Mask?	Description
DataCorruption	1003	No	Digital data corrupted, affecting low frac. of events
StuckBit	1002	No	Readout bit < 5 stuck at 0 or 1
LargeHfNoise	1100	No	RMS of the reconstructed amplitudes is large
CorrelatedNoise	1101	No	Noise among the ADC's is correlated
LargeLfNoise	1102	No	RMS of the first sample distribution is large
NoCis	1103	No	No CIS response
BadCis	1104	No	Measured CIS constant RMS/mean > 0.4%
GeneralMaskAdc	1000	Yes	Mask for problems not fitting any other description
AdcDead	1001	Yes	ADC is dead, reading out only 0 or pedestal value
VeryLargeHfNoise	1004	Yes	RMS of the reconstructed amplitudes is very large
NoData	1005	Yes	No data output from ADC
WrongDspConfig	1006	Yes	Online DSP config. used to collect data not correct
SevereStuckBit	1007	Yes	Readout bit > 4 stuck at 0 or 1
SevereDataCorruption	1008	Yes	Digital data is corrupted, affecting high frac. of events

Channel Status Flags

Flag	Flag#	Mask?	Description
NoLaser	2100	No	The PMT doesn't receive laser light
BadLaser	2101	No	PMT receives light but cannot be calibrated
NoCesium	2102	No	PMT doesn't respond to Cs scan
BadCesium	2103	No	PMT responds to Cs scan but cannot be calibrated
NoTiming	2104	No	Cannot set deskew timing delay for this PMT
BadTiming	2105	No	Time offset is not stable
GeneralMaskChannel	2000	Yes	Mask for problems not fitting any other description
NoPmt	2001	Yes	The PMT is not connected to the read-out or is dead
NoHV	2002	Yes	HV is not applied to the PMT
WrongHV	2003	Yes	Wrong HV applied to the PMT

Appendix

References

[1] *ATLAS tile calorimeter: Technical Design Report*, Technical Design Report ATLAS, CERN, 1996, URL: https://cds.cern.ch/record/331062.

[2] e. a. P. Adragna, *Testbeam studies of production modules of the ATLAS Tile Calorimeter*, Nuclear Instruments and Methods in Physics Research Section A: Accelerators, Spectrometers, Detectors and Associated Equipment **606** (2009) 362, ISSN: 0168-9002, URL: https://www.sciencedirect.com/science/article/pii/S016890020900792X.

[3] K. J. Anderson, M. H. Hurwitz, I. Jen-La Plante, J. E. Pilcher, and R. Teuscher, *Performance and Calibration of the TileCal Fast Readout Using the Charge Injection System*, tech. rep. ATL-TILECAL-INT-2008-002. ATL-COM-TILECAL-2008-003, CERN, 2008, URL: https://cds.cern.ch/record/1092929.

[4] A. T. Calorimeter, *ATLAS tile calorimeter data preparation for LHC first beam data taking and commissioning data*, Journal of Physics: Conference Series **219** (2010) 022030, URL: https://doi.org/10.1088%2F1742-6596%2F219%2F2%2F022030.

[5] K. Anderson et al., *Design of the front-end analog electronics for the ATLAS tile calorimeter*, Nucl. Instrum. Meth. **A551** (2005) 469.

[6] C. Berglund et al., *The ATLAS tile calorimeter digitizer*, tech. rep. ATL-TILECAL-PUB-2007-007. ATL-COM-TILECAL-2007-018, CERN, 2007, URL: https://cds.cern.ch/record/1071920.

[7] J. Dougherty et al., *Calibration Procedure For the ATLAS Tile Calorimeter Charge Injection System*, tech. rep. ATL-COM-TILECAL-2011-006, CERN, 2011, URL: https://cds.cern.ch/record/1334852.

List of contributions

Kathryn Chapman	
Jim Pilcher	Student supervision
Douglas Schaefer	Student supervision
Andrew Smith	Generated Run 2 CIS stability plots, helped organize information in the note.
Eleanor Rath	Editing note for accuracy